http://dx.doi.org/10.21577/0103-5053.20170209

J. Braz. Chem. Soc., Vol. 29, No. 4, 845-855, 2018.
Printed in Brazil - ©2018 Sociedade Brasileira de Química

Article

Synthesis, Characterization and Catalytic Evaluation of Magnetically Recoverable $SrO/CoFe_2O_4$ Nanocatalyst for Biodiesel Production from Babassu Oil Transesterification

Milton S. Falcão,[a] Marco A. S. Garcia,[a] Carla V. R. de Moura,[a] Sabrina Nicolodi[b] and Edmilson M. de Moura[*,a]*

[a]*Departamento de Química, Universidade Federal do Piauí (UFPI), 64049-550 Teresina-PI, Brazil*

[b]*Instituto de Física, Universidade Federal do Rio Grande do Sul (UFRGS), 91501-970 Porto Alegre-RS, Brazil*

Biodiesel production has gained a lot of attention due to its environmental benefits and production from renewable sources. Here, it is reported a magnetically recoverable catalyst of SrO immobilized on a $CoFe_2O_4$ support ($SrO/CoFe_2O_4$), which was efficiently applied for babassu oil transesterification and used up to four cycles without a significant activity loss. The stability and performance of the catalyst were analyzed considering the solvent used for its synthesis. Characterizations such as vibrating sample magnetometer (VSM), thermogravimetry (TG), X-ray diffraction (XRD), Fourier transform infrared spectroscopy (FTIR), scanning electron microscopy (SEM), transmission electron microscopy (TEM) and energy dispersive spectroscopy (EDS) were performed. The present study demonstrated that the catalyst has a strong magnetic response, which reflects the nature of the nanoparticles. For the first run, the material presented a yield of 96% when synthesized in acetone in a molar proportion of $SrO/CoFe_2O_4$ of 5:1.

Keywords: biodiesel, babassu oil, cobalt ferrite, strontium oxide

Introduction

The worldwide increasing energy demand, the fast petroleum shortage and other uncountable human-caused environmental pollutions are critical factors in the search for alternative energy supplies. The need for developing renewable energy sources without (or fewer) environmental effects is essential for future generations existence, and creating energy from low-carbon sources are key targets of researchers in the area.[1] Biodiesel has been recognized as an alternative fuel and a possible substitute for traditional energy sources due to its biodegradability and renewability.[2-4] Bearing that in mind, the production of an efficient catalyst is important, and magnetic supports are suggested as tools that allow circumventing difficulties in catalyst separation.[5-9] Ferrites are a class of ceramic compounds consisting of a mixture of several metal oxides with oxygen ions in a closed-packed structure with cations occupying its interstices.[5] Usually, the main constituent of ferrites is iron oxide and the well-known natural-occurring representative compound of these materials is magnetite, Fe_3O_4 ($Fe^{2+}O$, $Fe^{3+}O$). However, different ferrites may be derived from the aforementioned ferromagnetic material by replacing the divalent iron ion by another divalent ion from another metal, such as manganese, cobalt, nickel, zinc, calcium, magnesium and cadmium, or two different divalent ions at the same time.[10-12] Any ion substitution on the structure of ferrites may affect electrical and magnetic properties, nevertheless preparation conditions and porosity may influence the properties of the final materials as well.[13] The increasing development of nanoscience field allows the application of nanotechnology to improve ferrites applications on situations it was not conceivable years ago, such as on nanocatalysis.[14]

The application of easy-to-recover materials with surface-immobilized basic compounds is very pertinent to biodiesel production. Several studies have been made to add value to the modified agricultural obtained materials (i.e., vegetal oils) using chemical transformations in attempt to develop regional renewable products. Some investigations focus on the role of pure SrO and its mixture with small amounts of $SrCO_3$ and $Sr(OH)_2$ in transesterification

*e-mail: mmoura@ufpi.edu.br

reactions. De Moura *et al.*[15] studied the catalytic activity of pure SrO on babassu (*Attalea speciosa*) transesterification and Carvalho *et al.*[16] used a mixture of $SrCO_3$, SrO and $Sr(OH)_2$ in babassu and castor oil blends for biodiesel production. Both researchers obtained yields higher than 95% for the desired product, however, the troublesome catalysts separation was observed by either. Additionally, after the purification of the biodiesel produced, small amounts of the catalysts were still on it. If on one side decisions for catalysts applications on industry are closely related to its activity, in the other side separation processes may be considered on every unitary operation step and their efficiency must be maximum. Therefore, the studies show SrO as an excellent option for biodiesel production, but the separation from the reaction medium has to be simple and effective. The search for more stable catalysts and easier recoverable systems for biodiesel obtainment has been focus of intense investigation. Struggling to solve some difficulties, all sorts of heterogeneous catalysts step into the scene. In particular, catalytic magnetic supports have been studied lately and are very promising.[17-20] Many catalysts are presented in literature using the magnetic separation concept for different types of chemical reactions; however, examples with transesterification are still rare when compared to other reactions, as oxidations or hydrogenations.[5,17] Alves *et al.*[21] synthesized magnetic mixed iron/cadmium and iron/tin oxide nanoparticles which were active for hydrolysis and transesterification of soybean oil and esterification of its fatty acids. The most remarkable result was for esterification with the iron/tin system, which the yield reached ca. 84% in just 1 h and 200 °C. The catalyst was magnetically recovered and reused four times without loss of its activity.[21] Hu *et al.*[22] prepared KF/CaO-Fe_3O_4 as catalyst for transesterification of stillingia oil and obtained a yield of 95% in optimal conditions. Moreover, the magnetic catalyst was able to be reused up to 14 times without substantial activity loss and after all the separation procedures more than 90% of the material was recovered.[22] These two examples are among some others that present ferrites as key materials for separation procedures, encouraging new advances in the field.

Magnetic cobalt ferrite ($CoFe_2O_4$) nanoparticles have been considered lately[23,24] due to its thermal and chemical stability as core for heterogeneous nanocatalysts for photocatalysis,[25] phenol degradation,[26] acetylene decomposition for carbon nanotubes production,[27] for biomedical applications[28] and may be used as support of oxides for transesterification reactions of vegetable oil and fats.[23,24] Considering the vast range of applications that $CoFe_2O_4$ nanoparticles cover, different synthesis procedures are proposed to suit the material obtained with its usage. For magnetic supports, the co-precipitation method, which consists on the mutual precipitation of Fe^{3+} and Co^{2+} in a basic aqueous solution, is more likely to be used due to its simplicity;[29] however, it may result in a wide polydispersion of nanoparticles size which may affect their magnetic properties or interaction with the substrate.[30]

In continuation of our previous studies on the catalyst separation by a magnetic field, here it is reported the synthesis of $CoFe_2O_4$ using a co-precipitation method,[31,32] its characterization and all the features related to the application of the material as support for transesterification of babassu oil (*Orbignya phalerata*) using methanol as nucleophilic agent. Therefore, a wet impregnation procedure was performed with SrO onto the magnetic support, resulting in a material that was characterized and applied in catalytic experiments for activity improvement.

Experimental

Materials and methods

Analytical grade chemicals were purchased from Sigma-Aldrich and used without further purification: cobalt(II) chloride hexahydrate (≥ 97%), iron(III) chloride hexahydrate (≥ 97%), strontium(II) chloride hexahydrate (≥ 99%), anhydrous chloroform (≥ 99%), methanol (99.9%), ammonium hydroxide (28% NH_3 in water), hydrochloric acid (37%), acetone (≥ 99.9%) and methyl heptadecanoate (≥ 99%). Refined babassu oil was purchased at a local supermarket. The fatty acid composition of esters obtained from babassu oil is given in Table 1.

Table 1. Composition of babassu oil

Fatty acid	%
Caprylic acid (C8.0)	4.1
Capric acid (C10.0)	1.7
Lauric acid (C12.0)	45.0
Myristic acid (C14.0)	18.8
Palmitic acid (C16.0)	10.3
Stearic acid (C18.0)	2.3
Oleic acid (C18.1)	16.5
Linoleic acid (C18.2)	1.3

The magnetic characterization was performed by using an EZ9 MicroSense vibrating sample magnetometer (VSM) at room temperature with a magnetic field cycled between –22 and +22 kOe. Thermogravimetric (TG) measurements were performed on a DTG-60/DTG-60A Shimadzu equipment (TG/DTA (differential thermal analysis)

simultaneous measuring instrument). The experiments were conducted in the temperature range of 30 to 1100 °C using Pt crucible with approximately 15 mg of sample, heating rate of 10 °C min^{-1}, under dynamic nitrogen atmosphere (50 mL min^{-1}). The equipment conditions were verified with a standard reference of $CaC_2O_4{\cdot}H_2O$. The blank TG/DTG curves were obtained under the same experimental conditions for baseline correction. The X-ray diffractograms (XRD) were obtained using a Bruker D8 Advance equipment using monochromatic CuKα radiation (λ = 1.54056 Å) and graphite monochromator. The voltage of the copper emission tube was 40 kV and the filament current was 40 mA, at a 2θ range from 5° to 90° with a 0.02° step size and measuring time of 5 s *per* step. The spectra were acquired by Fourier transform infrared spectroscopy (FTIR) using a PerkinElmer Spectrum 100 GX FTIR System, set to measure 16 cumulative scans at 4 cm^{-1} in a range between 4000 and 400 cm^{-1}. The samples were prepared as KBr pellets.

The scanning electron microscopy (SEM) images were obtained using a ZEISS DSM 940A model operated at 15 kV. The samples were prepared by drop casting an isopropanol suspension containing the samples over a silicon wafer, followed by drying under ambient conditions. Transmission electron microscopy (TEM) images were obtained with a JEOL JEM 2100 microscope coupled to an energy-dispersive X-ray spectroscopy (EDS) device operating at 110 kV. Samples for TEM were prepared by drop casting an isopropanol suspension of the samples over a carbon-coated copper grid, followed by drying under ambient conditions. BET (Brunauer-Emmett-Teller) surface areas and pore size distribution on the materials were obtained on a Quantachrome Novawin equipment by N_2 physisorption at 77 K. Previously to the experiments, the catalyst was evacuated for 3 h at 150 °C to remove adsorbed water. The products were analyzed by using gas chromatography (GC, Shimadzu GC-2010 plus equipped with an Rtx-Wax capillary column and a flame ionization detector). The analyses were performed under the following conditions: constant column temperature of 250 °C with gas flow of 42.8 mL min^{-1} and pressure of 50.1 kPa. Flame ionization detector (FID) temperature was 250 °C.

Synthesis

Preparation of strontium oxide (SrO)

Strontium oxide was prepared by calcining $SrCO_3$. Strontium carbonate was prepared as following: 50 mL of an aqueous solution of $(NH_4)_2CO_3$ (1.0 mol L^{-1}) was mixed with 50 mL of an aqueous solution of $SrCl_2{\cdot}6H_2O$ (1.0 mol L^{-1}) and magnetically stirred for 60 min at 80 °C. The white powder of strontium carbonate formed was washed 3 times with water and dried at 100 °C for 24 h. The procedure for the SrO obtaining was simply to calcine $SrCO_3$ at 1100 °C for 180 min at a heating rate of 10 °C min^{-1}. The SrO was shortly used after its synthesis.[16]

Preparation of cobalt ferrite ($CoFe_2O_4$)

Cobalt ferrite magnetic nanoparticles were prepared by a co-precipitation method. An aqueous solution of $FeCl_3{\cdot}6H_2O$ (5 mL, 1.65 mol L^{-1}) was mixed with an aqueous solution of $CoCl_2{\cdot}6H_2O$ (5 mL, 1.65 mol L^{-1}) dissolved in HCl 2 mol L^{-1}. The solution prepared was added to 250 mL of ammonium hydroxide aqueous solution (0.7 mol L^{-1}) and mechanically stirred at 95 °C for 120 min in a reflux system. The black precipitate formed was cooled down to room temperature, collected with a permanent magnet and washed 3 times with distilled water and once with acetone. The solid was dried in a muffle furnace for 6 h at 120 °C and, then, calcined in atmospheric air at 800 °C in a heating rate of 10 °C min^{-1}.[33]

Preparation of catalyst ($SrO/CoFe_2O_4$)

A composite of strontium oxide and cobalt ferrite magnetic nanoparticles ($SrO/CoFe_2O_4$) was prepared using an impregnation method. SrO and $CoFe_2O_4$ were mixed in molar ratios of 1:1, 3:1, 4:1 and 5:1 under constant stirring in different solvents (water, methanol, ethanol or acetone) at 80 °C for 18 h using a reflux system. Then, the solid was collected with a permanent magnet, washed with the solvent used for its impregnation and dried in an oven at 120 °C for 6 h. The catalyst prepared was stored in an amber bottle.[33]

Catalytic experiments

Transesterification reactions were performed using a 100 mL distillation flask immersed in an oil bath coupled to a condensation system. In a typical reaction, the glass flask was loaded with catalyst and methanol and kept under continuous mechanical stirring for 20 min at 60 °C. Such initial step was performed just before the oil adding to increase the formation of the strong basic species CH_3O^-, which have high catalytic activity in the reaction.[34] Babassu oil was mixed to the former components in a molar ratio of 15:1 (methanol:oil). The amounts of methanol and oil used were based on the quantity of catalyst present in the first step, i.e., the experiments were planned to contain 4% of catalyst as a function of oil mass. The reaction was performed at 60 °C, for 3 h and 300 rpm of stirring. The catalyst was magnetically recovered by placing an $Nd_2Fe_{14}B$ magnet (well-known as neodymium magnet) on the flask wall for 2 min and the products were collected by simply

pouring them while the permanent magnet was being used. The used catalyst was washed once with acetone and once with chloroform, dried for 6 h at 120 °C in an oven and, then, calcined in a muffle furnace at 500 °C for 3 h at a heating rate of 10 °C min^{-1}.

The products were placed in a separatory funnel and washed three times with distilled water to remove glycerin, formed by a side reaction of the process, and unreacted methanol; afterward, the biodiesel was filtered through anhydrous sodium sulfate and stored in an amber flask. To analyze any SrO leaching, after each cycle, the catalyst was mixed with methanol and stirred at 3,000 rpm for 1 h at 60 °C. Then, the solid was removed by centrifugation at 3,500 rpm for 20 min and the residual methanol was added to babassu oil and the same reaction conditions were reproduced. The products were analyzed by GC analysis.

Identification and quantification of reaction products

Total fatty acid methyl esters (FAME) of refined babassu oil and its relative abundance were determined by GC according to retention times using standard products, or GC-MS (gas chromatography-mass spectrometry) spectra analysis, and the resulting information were compared to the current literature.[16,31] The conversion was calculated using methyl heptadecanoate as internal standard, according to our previous study based in international standards.[16] Approximately 100 mg of the samples were weighted and added to a chloroform solution of the internal standard in a concentration of 2.6 g L^{-1}. For the analysis, 1 μL of each sample was manually injected in the GC equipment.

Results and Discussion

Characterization

Spinel-type oxides show some benefits that make them suitable for being used as catalyst supports, e.g., good thermal and chemical stability, which prevent their dissolution in the reaction medium and, consequently, open up the possibility of their reutilization in successive catalytic cycles. Additionally, nanostructured magnetic materials are remarkable due to the magnetic separation efficiency from the reaction medium and its high surface area, which mostly increases the catalytic efficiency of a system.[32] Among all these advantages, it should be noticed that the performance of catalysts may be size-sensitive, i.e., the activity may increase with the decrease of particle size.[14] Cobalt compounds are usually cheaper than iron reagents, so its choice as Fe^{2+} replacement in the ferrite structure was straightforward and its influence on biodiesel production was motivating. Also, $CoFe_2O_4$ synthesis is very simple. The effect of SrO supported on the ferrite was the main goal of the studies performed, since the material is usually very active in transesterification reactions without (or fewer) soap formation.[34] Besides that, all the compounds used for the syntheses are quite accessible and inexpensive. To ensure the material chosen for the catalytic proposals of the study would meet all the above requirements, some characterizations were necessary.

The magnetic properties of the sample were evaluated by recording the magnetic field (H) dependence on the magnetization (M). The measurements were performed with a maximum magnetic field of 22 kOe (Hmax) at ambient temperature. According to Figure 1, the magnetic response of calcined $CoFe_2O_4$ and SrO/$CoFe_2O_4$ were basically the same, i.e., the immobilization of the oxide provides no significant change on the separation procedure adopted for the material. The magnetic signal of SrO/$CoFe_2O_4$ (M_{Hmax} ca. 14.6 emu g^{-1}) relative to the sample mass, decreases four times when matching it to $CoFe_2O_4$ response (M_{Hmax} ca. 58.5 emu g^{-1}); the reduction was expected due to the SrO impregnation, which was used in a molar ratio of 5:1 of SrO to cobalt ferrite. The relative remnant magnetization (M_R)/M_{Hmax} was approximately the same for both, corroborating the similarity of the magnetic parts of the samples, once again confirming the oxide immobilization does not affect its magnetic properties. The calcined $CoFe_2O_4$ and its immobilized counterpart, at room temperature, present coercive fields H_C = 510 and 620 Oe, respectively, and M_R/M_{Hmax} = 0.45. These values are expected for blocked relatively large particles of ca. 50 nm. However, it cannot be discarded the contribution of a reduced number of small size superparamagnetic particles, since magnetic saturation was not achieved with the 22 kOe field available. By normalizing the curves (not shown), it can be observed an almost similar shape. The slight alteration is attributed to changes of interacting effects among the magnetic particles. It is confirmed by observing SEM images of Figure 2, where the magnetic average inter-particle separation is evidently larger on the SrO-containing matrix.

For the immobilization process, the oxide was prepared from the strontium carbonate using a thermal decomposition approach. To guarantee the SrO formation, TG curves for the prepared $SrCO_3$ and for the as-synthesized $CoFe_2O_4$ (calcined at 800 °C) before and after immobilization of SrO are shown in Figure 3. All the experiments were conducted in temperature range of 30 to 1100 °C. For $SrCO_3$ (Figure 3a), there was a weight loss (Δm) event between 85 and 125 °C (Δm = 2.5%), due to adsorbed water elimination, and there was another weight loss between 895 and 1076 °C

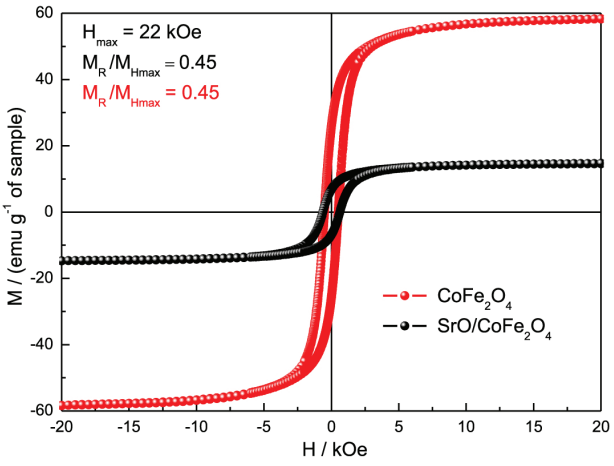

Figure 1. Magnetization curve of calcined $CoFe_2O_4$ and $SrO/CoFe_2O_4$ at room temperature.

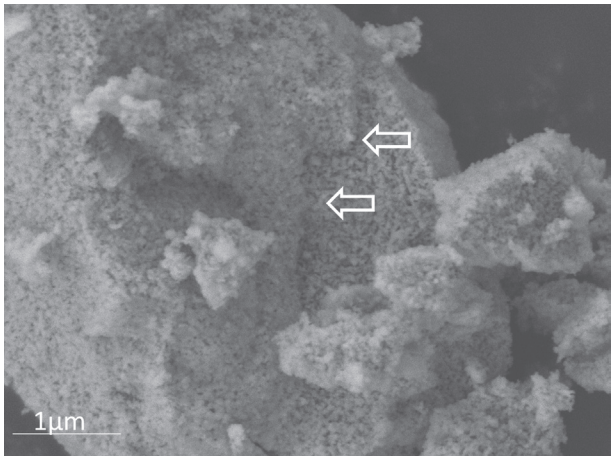

Figure 2. SEM image $SrO/CoFe_2O_4$ catalyst applied to the first cycle.

($\Delta m = 29.5\%$), which corresponds to $SrCO_3$ decomposition and SrO formation with CO_2 elimination. The second weight loss event justifies the temperature of calcination used for the SrO obtainment. For $CoFe_2O_4$ (Figure 3b), there was a weight loss event at the beginning of the curve. The event occurred between 30 and 124 °C and corresponded to physiosorbed water elimination ($\Delta m = 3.4\%$). Its apparent stability is a desirable property since transesterification catalysts, once applied to industrial routines, would endure cleaning and reactivation thermal processes. When the TG analysis of the $SrO/CoFe_2O_4$ catalyst itself was conducted (Figure 3c), there was a continuous and truly discrete weight loss up to 140 °C, due to some atmospheric water adsorption. However, there is an intense weight loss ($\Delta m = 21.2\%$) between the temperature of 351 to 412 °C, which corresponds to $Sr(OH)_2$ decomposition since SrO is high hydroscopic, which promotes the hydroxide formation.[35]

The $CoFe_2O_4$ (Figure 4) synthesis was confirmed by X-ray diffraction, using the Joint Committee on Powder Diffraction Standard (JCPDS) crystallographic patterns,

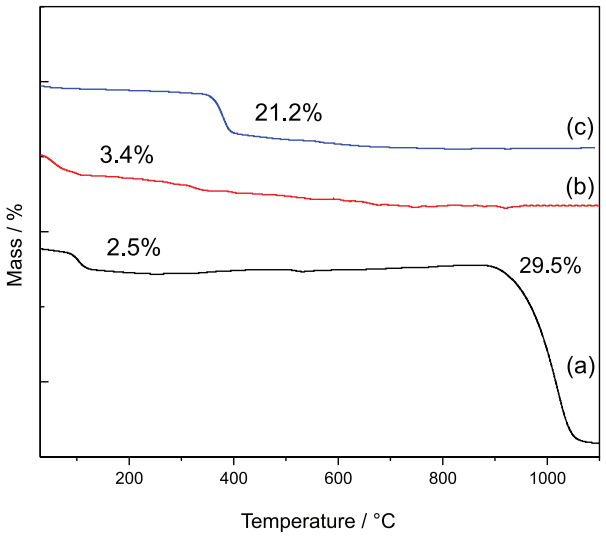

Figure 3. TG curves of (a) $SrCO_3$; (b) $CoFe_2O_4$ calcined at 800 °C and (c) $SrO/CoFe_2O_4$.

available at Crystallographica Search Match software. Basically, the diffractogram pattern of the calcined $SrCO_3$ (Figure 4c) was indexed for SrO, $Sr(OH)_2$ and $SrCO_3$, which corroborates the oxide formation (JCPDS 6-520). However, the pattern clearly shows the crystalline phases of some partially not decomposed $SrCO_3$ (JCPDS 5-418) and $Sr(OH)_2$ (JCPDS 74-407), spontaneously formed due to the atmospheric humidity. The pattern of the calcined $CoFe_2O_4$ (JCPDS 22-1086) visibly shows formation of a high crystallinity phase. It may be attested due to sharper and pronounced peaks when compared with the as-synthesized and not calcined sample (Figures 4a and 4b).[36,37] No other patterns were found on the $CoFe_2O_4$ sample, which demonstrate the efficiency of the co-precipitation method of synthesis.

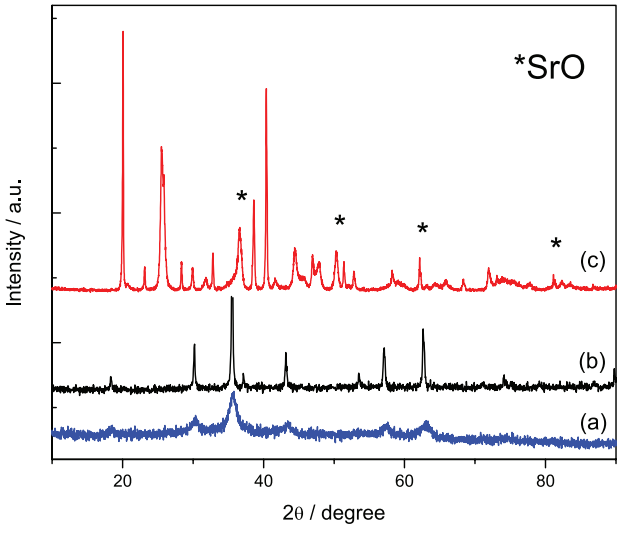

Figure 4. Diffractogram patterns of $CoFe_2O_4$ (a) not calcined; (b) calcined at 800 °C and (c) $SrCO_3$ (calcined at 1100 °C).

The as-synthesized SrO sample was also analyzed by FTIR. The infrared spectrum presents bands at 592 and 448 cm^{-1}, associated with Sr–O stretching, confirming the SrO formation and validating the TG and XRD information obtained before. Other two medium stretching bands at 3612 and 3499 cm^{-1} (hydrogen bonds and free hydroxyl, respectively) and a weak stretching band at 1628 cm^{-1} could be observed, suggesting $Sr(OH)_2$ formation. C=O bond stretching at 1448 and 901 cm^{-1} are evident in the sample, indicating some carbonate from $SrCO_3$ (Figure 5a).[14] The presence of water was confirmed by the technique, as well as for TG and X-ray methods. In the FTIR spectrum for the ferrite (Figure 5b), the weak bands at 3523, 3443 and 1629 cm^{-1} are related to water adsorbed on the material surface. The bands at approximately 582 and 402 cm^{-1} are assigned to metal-oxygen interactions; however, the former is a tetrahedral interaction and the other is an octahedral one.[38,39] The catalyst SrO/$CoFe_2O_4$ (Figure 5c) presents bands at 587 and 418 cm^{-1}, which are attributed to SrO, and stretching bands at 1633, 3613, 3500 cm^{-1}, typically attributed to O–H, suggesting $Sr(OH)_2$ formation. A strong band (1448 cm^{-1}) and a medium one (901 cm^{-1}) characterize carbonyl from $Sr(CO_3)_2$. Matching the bands of the as-synthesized ferrite with the SrO immobilized sample, small displacements are observed; they are ascribed to polarity increasing of metal-oxygen bonds.[37,40] All the information here described is important for the catalytic activity explanations, as seem ahead.

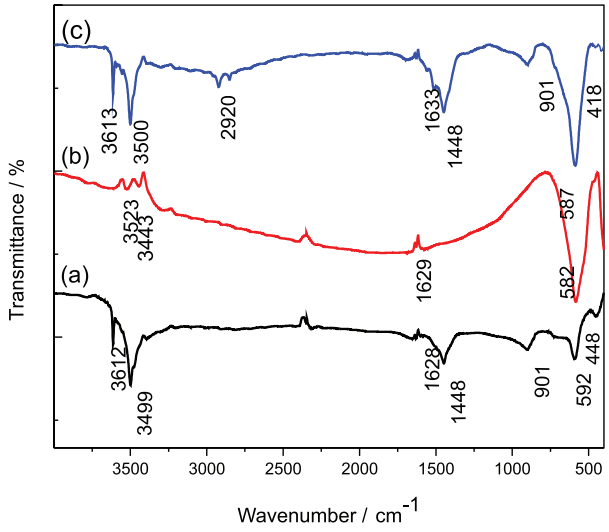

Figure 5. FTIR spectra of (a) $SrCO_3$ calcined at 1100 °C; (b) $CoFe_2O_4$ calcined at 800 °C and (c) SrO/$CoFe_2O_4$.

Considering the ferrite is nanostructured, as suggested by the magnetic properties obtained, a good practice to examine its shape, as well as the strontium immobilized, is performing microscopy analyses on the material. Figure 6 shows SEM and TEM images of calcined cobalt ferrite at 800 °C. SEM image (Figure 6a) clearly displays particles with an irregular laminar surface, resulting from sintering process caused by calcination. TEM image (Figure 6b) corroborates the observed result since darker or lighter points on the structure are seen due to overlapping of a different number of cobalt ferrite layers. The presence of light structures indicates that there are few overlapping structures, whereas the intensification of the dark tonality indicates a gradual increase of structures overlapping.[40]

The sample was suitable for energy dispersive spectroscopy (EDS) and the process was performed during TEM analysis. The results are presented in Figure 7 and match to the circles A to E represented in Figure 6. The spots present the same chemical composition with concentrations of cobalt, iron and oxygen increasing in the flowing series: C < D < B < A < E. The F circle shows no EDS signal related to the elements of interest. The elemental chemical composition of cobalt ferrite obtained from the EDS data (Table 2) suggests a minimum formula

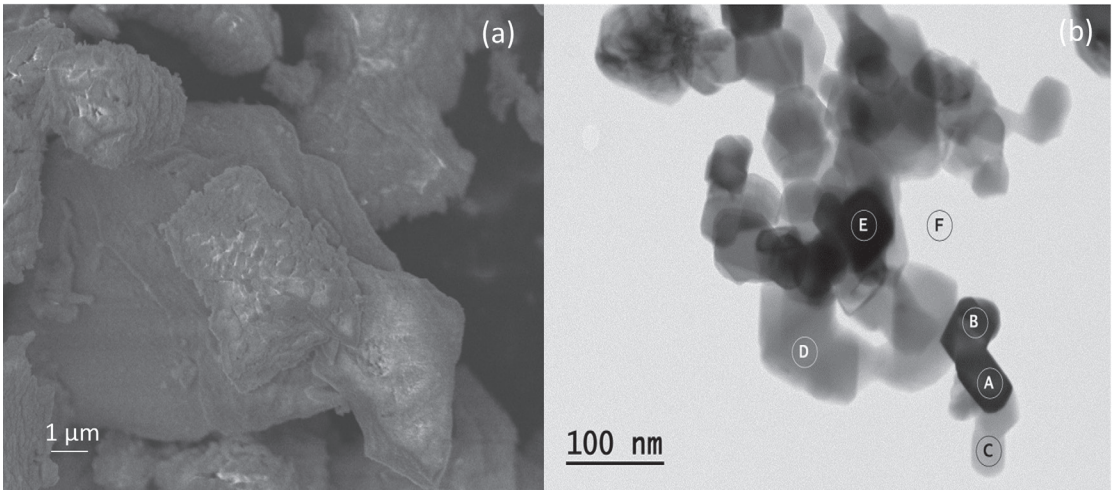

Figure 6. (a) SEM and (b) TEM images of $CoFe_2O_4$ particles calcined at 800 °C. The circles A to F represent the spots analyzed by EDS.

of $Co_{1.00}Fe_{2.00}O_{4.13}$. The composition obtained agree with the data presented by Senapati *et al.*[37]

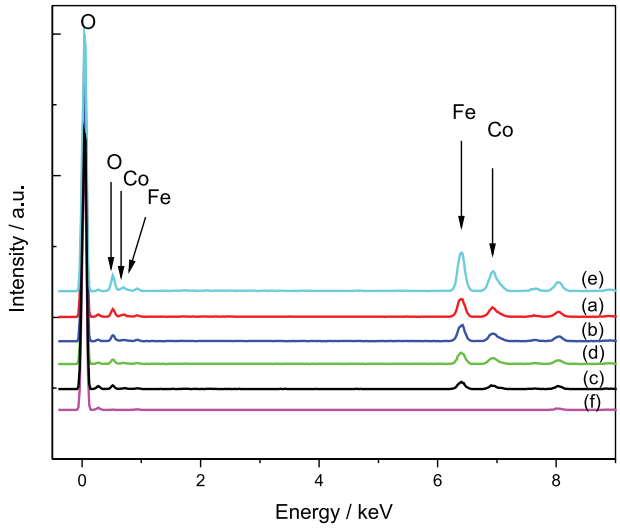

Figure 7. EDS data of $CoFe_2O_4$ calcined at 800 °C. (a-f) match the circles A to F represented in Figure 6.

Table 2. Elemental composition of $CoFe_2O_4$

Element	Atomic count					
	A	B	C	D	E	Average
O	1647	1654.4	1011.0	2374.3	5607.3	2458.80
Fe	398.8	400.6	244.8	574.9	1357.7	595.36
Co	201.3	208.6	116.1	268.4	692.4	297.36
O/Fe	–	–	–	–	4.129	–
Fe/Co	–	–	–	–	2.002	–

A-E: match the atomic count obtained by using EDS data.

SEM image (Figure 2) of the as-prepared catalyst presents arrows which display junctions of cobalt ferrite due to its laminar surface, as seen before. Small particles of strontium oxide are all over the surface of the ferrite. The $CoFe_2O_4$ BET analysis indicates a well-developed pore structure with a significant pore volume value (3.61 $cm^3\ g^{-1}$) and a large surface area (10.22 $m^2\ g^{-1}$), which are essential requirements for the activity of a catalyst. The SrO/$CoFe_2O_4$ catalyst presented a surface area of 4.36 $m^2\ g^{-1}$ with a pore volume of 1.54 $cm^3\ g^{-1}$. The reduction on the surface and volume parameters was caused by the strontium oxide immobilization, that is in accordance to SEM image, which shows the impregnation of SrO across the entire $CoFe_2O_4$ surface, suggesting pore filling by part of the strontium compound. It is expected strong interactions between the two oxides, according to studies performed before.[33] The catalyst recycling and catalyst synthesis solvent choice cast light on this matter and are further discussed.

Improvement of the catalyst performance

All the reactions were performed using a molar ratio of methanol:oil of 15:1, 4% of catalyst (based on the mass of oil used), 60 °C and 3 h of reaction under continuous stirring. The solvent used for the impregnation process of SrO on the magnetic material considerably affects the physicochemical properties of the material. When water is used as solvent, part of the oxide solubilizes, so only a small amount was able to be immobilized on the support with hydroxide formation, requiring calcination at 500 °C for 3 h before the catalytic activity test, in order to decompose $Sr(OH)_2$, transforming the entire procedure in a time-consuming process. However, the catalyst prepared in water essentially maintained the activity for the second run (Table 3), suggesting the calcination process contributes to the oxide immobilization on the magnetic nanoparticles. The reduced activity is related to the SrO:$CoFe_2O_4$ ratio change due to dissolution of part of strontium material. Methanol and ethanol produce soluble strontium compounds (methoxide and ethoxide, respectively), which modifies the planned catalyst molar ratio; SrO is insoluble in acetone and provided full strontium oxide uptake, maintaining the desired molar ratio of SrO to support.

Table 3. Solvent effect on the SrO immobilization[a]

Solvent	1st cycle / %	2nd cycle / %
Water	56 ± 2.5	51 ± 2.0
Methanol	97 ± 0.9	44 ± 2.8
Ethanol	74 ± 1.5	51 ± 2.0
Acetone	96 ± 0.9	77 ± 2.4

[a]Temperature: 60 °C; mass percentage of catalyst: 4; methanol:oil molar ratio: 15:1; reaction time: 3 h.

The effect of the calcination was also investigated. Table 3 shows the performance of the catalysts synthesized in different solvents in transesterification reactions of babassu oil after calcination. The catalyst synthesized with water as solvent presented a similar activity in cycles 1 and 2, however, they were not very high. The calcination process may have caused agglomeration of the particles. The performances of the catalysts impregnated in methanol and ethanol presented remarkable reductions between the first and second cycles, due to pronounced leaching, which was visible to the eye by the turbidity of the produced biodiesel. The yield of 96% may be explained by the catalyzed transesterification mechanism for SrO. After calcination, the catalyst prepared in acetone provided a significant activity in the first cycle, maintaining 77% of the activity in the second run. SrO and $CoFe_2O_4$ are

insoluble and inert in acetone, which makes the solvent appropriate for the impregnation process, maintaining the theoretically predicted chemical proportion, significantly reducing the level of leaching in each cycle and allowing the obtainment of a product with levels of contamination within the standards of quality demanded by international establishments.

Another synthetic pathway studied refers to the molar ratio of SrO/$CoFe_2O_4$. The catalyst was synthesized using four different proportions of the oxide and ferrite and its catalytic action was evaluated in order to define the best composition. Table 4 shows the catalytic performance of SrO/$CoFe_2O_4$ in the transesterification of babassu oil under the same conditions (temperature, catalyst percentage, reaction time), except for the methanol:oil molar ratio. Increasing the amount of impregnated SrO improved the reaction yield to the limit of 5:1. From the molar ratio 1:1 to 5:1 (SrO/$CoFe_2O_4$), there was a significant yield improvement. At the molar ratio 1:1, the yield was very irrelevant, probably due to a poor coverage of the ferrite. The increasing molar ratio clearly follows a trend of activity augmentation, however, the best proportion was the 5:1 due to its higher yield. Other increasing ratio would be pointless since any enhancement would be very discrete and would not explain any more SrO usage.

Table 4. SrO/$CoFe_2O_4$ molar ratio effect on the babassu oil transesterification yield[a]

Catalyst	Proportion of SrO/$CoFe_2O_4$	Yield / %
SCF11	1:1	12 ± 2.6
SCF31	3:1	78 ± 1.5
SCF41	4:1	93 ± 1.2
SCF51	5:1	96 ± 0.9

[a]Temperature: 60 °C; mass percentage of catalyst: 4; methanol:oil molar ratio: 15:1; reaction time: 3 h.

Catalytic activity and recyclability

Gathering all the catalytic and characterization data obtained, the best synthetic pathway was selected: $CoFe_2O_4$ immobilized with SrO on acetone medium in a molar ratio of 5:1 (SrO/$CoFe_2O_4$). Any further physicochemical details were published elsewhere.[41] The babassu oil composition was evaluated by using GC and the products were analyzed by comparison of the retention times with analytical standards or by GC-MS spectra analysis. The results of oil composition as well as its percentage are shown in Table 1. The babassu biodiesel is comprised of 82.2% of saturated compounds and up to 69.6% of esters from fatty acids of short chain (8 to 14 carbons). Materials with such composition present low viscosity, high volatility and good oxidative stability; features highly desirable for commercial applications.[42]

Data on the transesterification reaction of babassu are given in Figure 8. The reaction at 60 °C occurred in 3 h with high activity for the first run (96%), albeit its yield decreased run by run (65% for the fourth run). Although activity after 4 cycles was observed, its reduction must be considered. Yoo *et al.*[43] suggests part of the strontium reacts with methanol and forms $Sr(OCH_3)_2$, proposing leaching of the metal in each run, what would break the optimum molar ratio of the material as well as reduce metal over the ferrite surface. However, the heterogeneity test demonstrated the contribution of the homogeneous phase of the catalyst to the transesterification reaction was very low in all cycles; the results of gas chromatography analyses for ester conversion were lower than 5% and, therefore, do not directly contribute to reduction of activity between cycles. Tests confirm that the cleaning step did not contribute to any leaching as well. Another explanation for the reduction of activity was the formation of strontium hydroxide. The compound is 17 times more soluble in methanol than strontium oxide, which would cause, again, some leaching and decrease of efficiency.[15,44] The hydroxide would be dissolved in glycerol, a common byproduct in biodiesel industry. The formation of $Sr(OH)_2$ was attested by FTIR, XRD and TG, as seen before. Among others, the sintering is something possible in each run and may interfere in the effectiveness of the catalyst. BET analysis demonstrated a reduction of the surface area of the catalyst used in the fourth cycle when compared to the first.

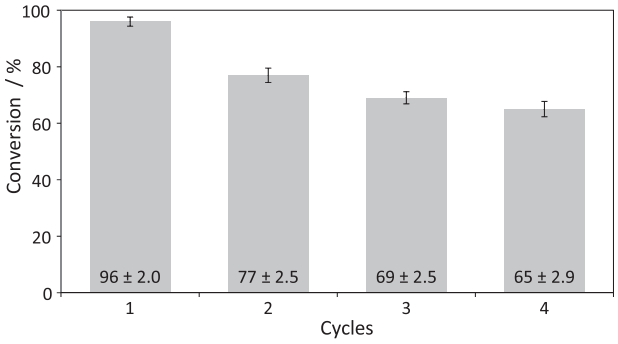

Figure 8. Comparison of the yield obtained in 4 different runs using the optimized SrO/$CoFe_2O_4$ catalyst.

To shed some light on the problem, XRD experiments were performed after each run (Figure 9). One may observe the diffractogram pattern indexed for $Sr(OH)_2$ are not visible after the first run. Clearly the absence of the pattern is connected to the calcination process performed after each

cycle at 500 °C, what makes the methodology mandatory, as seen in the diffractograms. The pattern indexed to SrO is present in all the diffractograms; however, some crystallite changes occurred since the peaks width varied from the first diffractogram to the second one, although any clear modification was observed among the diffractograms of the second, third and fourth runs. Even after the fourth cycle and all the calcinations the material underwent, strontium carbonate was constantly present. Although $Sr(OH)_2$ does not affect the catalyst performance,[16] part of the strontium on the catalyst is not active due to $Sr(OH)_2$ existence.

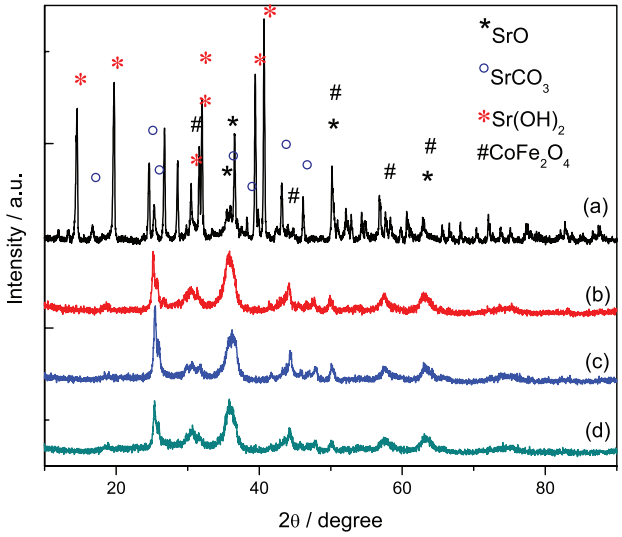

Figure 9. XRD diffractograms of catalyst $SrO/CoFe_2O_4$: (a) first, (b) second, (c) third and (d) fourth runs.

The diffractogram proved that there was a sintering process during the cycles. In SEM image (Figure 10) it is possible to observe a granule irregular surface, apparently composed of smaller sintered structures, probably caused by the routine of calcination to which the catalyst was submitted before each reuse. The process certainly resulted from the calcination methodology applied for the catalyst recycling. According to BET data, after the fourth run, the superficial area and the pore volume increased. The superficial area increased from 4.36 to 8.40 $m^2\ g^{-1}$ and the pore volume from 1.54 to 3.38 $cm^3\ g^{-1}$. Data suggest leaching of the impregnated oxide, cleaning the oxide surface.

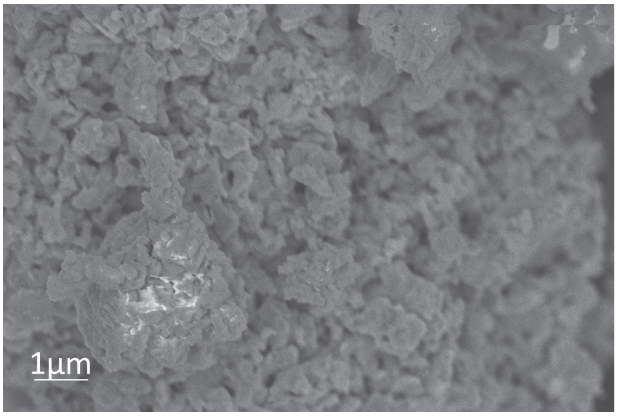

Figure 10. SEM image of $SrO/CoFe_2O_4$ catalyst after the fourth run.

Even though the catalyst cleaning and reactivation methodology exhibited the inconvenient effect of agglomeration of the catalyst particles, with a direct consequence on the yield of the transesterification reaction, the procedure was necessary and of great importance, since the presence of reagent/product from previous reaction cycles, especially glycerol, would interfere on the performance of the catalyst when applied in subsequent cycles, thus reducing the yield of the reaction.[45] The catalyst reactivation methodology promotes the removal of hydrophilic and hydrophobic compounds from the surface of the material allowing it to remain accessible to reagents in the following reaction cycles. The recycling tests performed by simply methanol washing after each reaction cycle presented yields lower than 40% from the second run on, reaching a yield of 3.4% in the fourth cycle. In the case of catalysts based on strontium oxide, not immobilized, Chen *et al.*[46] described that the loss of catalytic activity may be attributed to the formation of soap, from the reaction of the oxide with free fatty acids present in the oil. In the first cycle, the amount of soap formed is not sufficient to cover all the active sites; however, already in the second cycle, the soap formed can completely cover the remaining active sites resulting in the complete loss of catalytic activity.

Conclusions

A magnetic support was easily prepared by a co-precipitation method and further modified with SrO immobilization using a wet-impregnation approach. The evaluation of the synthesis conditions showed an important influence of the solvent on the process of immobilization of the oxide on the magnetic support. Among many characterizations performed, the magnetic properties confirmed that the magnetic response was basically the same for bare support and for the SrO-immobilized, an important feature for easy separation/re-dispersion of the material once it was necessary. The proposed method for the immobilization of the strontium oxide was shown to be simple and efficient. Microscopy images associated to EDS data sustained an elemental composition proposal for the ferrite support. The best catalytic activity for methanolysis reaction of babassu oil was observed for the catalyst synthesized in acetone at the $SrO/CoFe_2O_4$ ratio of 5:1, with

a yield of 96% of methyl esters. The catalyst was used in four successive cycles; it was submitted to a simple, fast and low-cost reactivation process and maintained a high yield for the transesterification reaction. XRD were used to analyze the strontium species existence after the catalytic runs and suggested a $Sr(OH)_2$ depletion over the cycles.

Acknowledgments

The authors are grateful to the Brazilian government agencies FAPEPI and CNPq for financial support.

References

1. Ma, F.; Hanna, M. A.; *Bioresour. Technol.* **1999**, *70*, 1.
2. Aransiola, E. F.; Ojumu, T. V.; Oyekola, O. O.; Madzimbamuto, T. F.; Ikhu-Omoregbe, D. I. O.; *Biomass Bioenergy* **2014**, *61*, 276.
3. Farias, A. F. F.; da Conceição, M. M.; Cavalcanti, E. H. S.; Melo, M. A. R.; dos Santos, I. M. G.; de Souza, A. G.; *J. Therm. Anal. Calorim.* **2016**, *123*, 2121.
4. Medeiros, M. L.; Cordeiro, A. M. M. T.; Queiroz, N.; Soledade, L. E. B.; Souza, A. L.; Souza, A. G.; *Energy Fuels* **2014**, *28*, 1074.
5. Rossi, L. M.; Garcia, M. A. S.; Vono, L. L. R.; *J. Braz. Chem. Soc.* **2012**, *23*, 1959.
6. Chen, C.-T.; Dutta, S.; Wang, Z.-Y.; Chen, J. E.; Ahamad, T.; Alshehri, S. M.; Yamauchi, Y.; Lee, Y.-F.; Wu, K. C. W.; *Catal. Today* **2016**, *278*, 330.
7. Raita, M.; Arnthong, J.; Champreda, V.; Laosiripojana, N.; *Fuel Process. Technol.* **2015**, *134*, 189.
8. Kharisov, B. I.; Dias, H. V. R.; Kharissova, O. V.; *Arab. J. Chem.* **2014**, DOI 10.1016/j.arabjc.2014.10.049.
9. Wang, H.; Covarrubias, J.; Prock, H.; Wu, X.; Wang, D.; Bossmann, S. H.; *J. Phys. Chem. C* **2015**, *119*, 26020.
10. Neelakanta, P. S.; *Handbook of Electromagnetic Materials: Monolithic and Composite Versions and Their Applications*, 1st ed.; CRC Press: Boca Raton, USA, 1995.
11. Hajalilou, A.; Mazlan, S. A.; *Appl. Phys. A* **2016**, *122*, 680.
12. Mohallem, N. D. S.; Silva, J. B.; Nascimento, G. L. T.; Guimarães, V. L. In *Nanocomposites - New Trends and Developments*, 1st ed.; Ebrahimi, F., ed.; InTech: Austria, 2012, ch. 18.
13. Tudorache, F.; Petrila, I.; *J. Electron. Mater.* **2014**, *43*, 3522.
14. Philippot, K.; Serp, P.; *Nanomaterials in Catalysis*, 1st ed.; Serp, P.; Philippot, K., eds.; Wiley-VCH Verlag GmbH & Co. KGaA: Weinheim, Germany, 2013, ch. 1.
15. de Moura, C. V. R.; de Castro, A. G.; de Moura, E. M.; dos Santos, J. R.; Moita Neto, J. M.; *Energy Fuels* **2010**, *24*, 6527.
16. Carvalho, L. M. G.; Abreu, W. C.; Silva, M. G. O.; Lima, J. R. O.; Oliveira, J. E.; Matos, J. M. E.; Moura, C. V. R.; Moura, E. M.; *J. Braz. Chem. Soc.* **2013**, *24*, 550.
17. Rossi, L. M.; Costa, N. J. S.; Silva, F. P.; Wojcieszak, R.; *Green Chem.* **2014**, *16*, 2906.
18. Matsuda, H.; Ito, T.; Kuchar, D.; Tanahashi, N.; Watanabe, C.; *Chemosphere* **2009**, *74*, 1348.
19. Thatai, S.; Khurana, P.; Boken, J.; Prasad, S.; Kumar, D.; *Microchem. J.* **2014**, *116*, 62.
20. Ho, K.-C.; Chen, C.-L.; Hsiao, P.-X.; Wu, M.-S.; Huang, C.-C.; Chang, J.-S.; *Energy Procedia* **2014**, *61*, 1302.
21. Alves, M. B.; Medeiros, F. C. M.; Sousa, M. H.; Rubim, J. C.; Suarez, P. A. Z.; *J. Braz. Chem. Soc.* **2014**, *25*, 2304.
22. Hu, S.; Guan, Y.; Wang, Y.; Han, H.; *Appl. Energy* **2011**, *88*, 2685.
23. Zhang, P.; Han, Q.; Fan, M.; Jiang, P.; *Appl. Surf. Sci.* **2014**, *317*, 1125.
24. Zhang, Y.; Yan, B.; Ou-Yang, J.; Zhu, B.; Chen, S.; Yang, X.; Liu, Y.; Xiong, R.; *Ceram. Int.* **2015**, *41*, 11836.
25. Huang, S.; Xu, Y.; Xie, M.; Xu, H.; He, M.; Xia, J.; Huang, L.; Li, H.; *Colloids Surf., A* **2015**, *478*, 71.
26. Shi, B.-N.; Wan, J.-F.; Liu, C.-T.; Yu, X.-J.; Ma, F.-W.; *Mater. Sci. Semicond. Process.* **2015**, *37*, 241.
27. Khedr, M. H.; Bahgat, M.; Abdel-Moaty, S. A.; *J. Anal. Appl. Pyrolysis* **2009**, *84*, 117.
28. Amiri, S.; Shokrollahi, H.; *Mater. Sci. Eng., C* **2013**, *33*, 1.
29. Bhattacharyya, S.; Salvetat, J.-P.; Fleurier, R.; Husmann, A.; Cacciaguerra, T.; Saboungi, M.-L.; *Chem. Commun.* **2005**, 4818.
30. Garcia, M. A. S.; Teruya, L. C.; Yoshimoto, K. M.; Rossi, L. M.; Di Vitta, P. B.; *Sep. Sci. Technol.* **2017**, *52*, 504.
31. de Caland, L. B.; Santos, L. S. S.; de Moura, C. V. R.; de Moura, E. M.; *Catal. Lett.* **2009**, *128*, 392.
32. Guin, D.; Baruwati, B.; Manorama, S. V.; *J. Mol. Catal. A: Chem.* **2005**, *242*, 26.
33. de Moura, E. M.; Garcia, M. A. S.; Gonçalves, R. V.; Kiyohara, P. K.; Jardim, R. F.; Rossi, L. M.; *RSC Adv.* **2015**, *5*, 15035.
34. Liu, X.; He, H.; Wang, Y.; Zhu, S.; *Catal. Commun.* **2007**, *8*, 1107.
35. Dias, A. P. S.; Bernardo, J.; Felizardo, P.; Correia, M. J. N.; *Fuel Process. Technol.* **2012**, *102*, 146.
36. Gyergyek, S.; Drofenik, M.; Makovec, D.; *Mater. Chem. Phys.* **2012**, *133*, 515.
37. Senapati, K. K.; Borgohain, C.; Phukan, P.; *J. Mol. Catal. A: Chem.* **2011**, *339*, 24.
38. Albuquerque, A. S.; Tolentino, M. V. C.; Ardisson, J. D.; Moura, F. C. C.; de Mendonça, R.; Macedo, W. A. A.; *Ceram. Int.* **2012**, *38*, 2225.
39. Gherca, D.; Pui, A.; Nica, V.; Caltun, O.; Cornei, N.; *Ceram. Int.* **2014**, *40*, 9599.
40. Borgohain, C.; Senapati, K. K.; Sarma, K. C.; Phukan, P.; *J. Mol. Catal. A: Chem.* **2012**, *363-364*, 495.
41. de Abreu, W. C.; de Moura, C. V. R.; Costa, J. C. S.; de Moura E. M.; *J. Braz. Chem. Soc.* **2017**, *28*, 319.

42. Kumar, N.; *Fuel* **2017**, *190*, 328.
43. Yoo, S. J.; Lee, H.-S.; Veriansyah, B.; Kim, J.; Kim, J.-D.; Lee, Y.-W.; *Bioresour. Technol.* **2010**, *101*, 8686.
44. Jiao, Y.; Wang, J.; Qin, L.; Wang, J.; Zhu, Q.; Li, X.; Gong, M.; Chen, Y.; *Chin. J. Catal.* **2013**, *34*, 1139.
45. Viola, E.; Blasi, A.; Valerio, V.; Guidi, I.; Zimbardi, F.; Braccio, G.; Giordano, G.; *Catal. Today* **2012**, *179*, 185.
46. Chen, C.-L.; Huang, C.-C.; Tran, D.-T.; Chang, J.-S.; *Bioresour. Technol.* **2012**, *113*, 8.

Submitted: September 6, 2017
Published online: November 27, 2017

FAPERGS/CAPES has sponsored the publication of this article.